Revisiting the Lower Bound on Tidal Deformability Derived by AT 2017gfo

Kenta Kiuchi[1,2] , Koutarou Kyutoku[2,3,4,5] , Masaru Shibata[1,2] , and Keisuke Taniguchi[6]

[1] Max Planck Institute for Gravitational Physics (Albert Einstein Institute), Am Mühlenberg 1, Potsdam-Golm D-14476, Germany
[2] Center for Gravitational Physics, Yukawa Institute for Theoretical Physics, Kyoto University, Kyoto, 606-8502, Japan
[3] Theory Center, Institute of Particles and Nuclear Studies, KEK, Tsukuba 305-0801, Japan
[4] Department of Particle and Nuclear Physics, the Graduate University for Advanced Studies (Sokendai), Tsukuba 305-0801, Japan
[5] Interdisciplinary Theoretical and Mathematical Sciences Program (iTHEMS), RIKEN, Wako, Saitama 351-0198, Japan
[6] Department of Physics, University of the Ryukyus, Nishihara, Okinawa 903-0213, Japan

Abstract

We revisit the lower bound on binary tidal deformability $\tilde{\Lambda}$ imposed by a luminous kilonova/macronova, AT 2017gfo, by numerical-relativity simulations of models that are consistent with gravitational waves from the binary neutron star merger GW170817. Contrary to the claim made in the literature, we find that binaries with $\tilde{\Lambda} \lesssim 400$ can explain the luminosity of AT 2017gfo, as long as moderate mass ejection from the remnant is assumed as had been done in previous work. The reason is that the maximum mass of a neutron star is not strongly correlated with the tidal deformability of neutron stars with a typical mass of $\approx 1.4\,M_\odot$. If the maximum mass is so large that the binary does not collapse into a black hole immediately after merger, the mass of the ejecta can be sufficiently large irrespective of the binary tidal deformability. We present models of binary mergers with $\tilde{\Lambda}$ down to 242 that satisfy the requirement on the mass of the ejecta from the luminosity of AT 2017gfo. We further find that the luminosity of AT 2017gfo could be explained by models that do not experience bounce after merger. We conclude that the luminosity of AT 2017gfo is not very useful for constraining the binary tidal deformability. Accurate estimation of the mass ratio will be necessary to establish a lower bound using electromagnetic counterparts in the future. We also caution that merger simulations that employ a limited class of tabulated equations of state could be severely biased due to the lack of generality.

Key words: equation of state – gravitational waves – stars: neutron

1. Introduction

The first binary neutron star merger was observed as the multi-messenger event GW170817/GRB 170817A/AT 2017gfo (Abbott et al. 2017b, 2017c, 2017d). Gravitational and electromagnetic signals have been combined to derive various information about physics and astrophysics. Examples include the velocity of gravitational waves (Abbott et al. 2017b), Hubble's constant (Abbott et al. 2017a), the central engine of a type of short gamma-ray burst (Mooley et al. 2018), and the origin of (at least a part of) r-process elements (Kasen et al. 2017; Tanaka et al. 2017).

The multi-messenger observations also constrain properties of neutron stars. Gravitational waves, GW170817, constrain the so-called binary tidal deformability to $100 \lesssim \tilde{\Lambda} \lesssim 800$, where precise values depend on the method of analysis and adopted theoretical waveforms (Abbott et al. 2018, 2019; De et al. 2018). At the same time, some researchers have argued that the maximum mass of a neutron star M_{max} cannot be significantly larger than ≈ 2.15–$2.2\,M_\odot$ based on the electromagnetic features, e.g., the absence of magnetar-powered radiation (Margalit & Metzger 2017; Shibata et al. 2017; Rezzolla et al. 2018; Ruiz et al. 2018). Bauswein et al. (2017) also proposed lower bounds on the radii of massive neutron stars, assuming that the electromagnetic signals may imply the avoidance of the prompt collapse. These inferences suggest that supranuclear-density matter is unlikely to be very stiff.

Radice et al. (2018b) proposed a novel idea: $\tilde{\Lambda} \gtrsim 400$ is required to eject material heavier than $0.05\,M_\odot$, which the

authors assumed to be required by the high luminosity of AT 2017gfo.[7] The logic is that no binary model with $\tilde{\Lambda} \lesssim 400$ is capable of ejecting $0.05\,M_\odot$, even if all of the baryonic remnant can be ejected, in their numerical-relativity simulations performed with four tabulated equations of state derived by mean-field theory. This constraint approximately indicates that neutron stars must be larger than 12 km (Zhao & Lattimer 2018), and thus it could reject mildly soft equations of state if reliable. Indeed, this constraint has been used to infer properties of nuclear matter by various researchers (Burgio et al. 2018; Lim & Holt 2018; Malik et al. 2018; Most et al. 2018). Later, Radice & Dai (2019) loosened the limit to $\tilde{\Lambda} \gtrsim 300$ by Bayesian inferences; they allowed a standard deviation of 50% in the fitting formula of disk masses, which they required to be $>0.04\,M_\odot$, derived using results of Radice et al. (2018b). Coughlin et al. (2018a) also derived a lower limit of $\tilde{\Lambda} \gtrsim 279$ by Bayesian inferences, with the improvement of the fit of disk masses via incorporation of the ratio of the total mass to the threshold mass for the prompt collapse as an additional parameter. Note that these two works also use other signals, such as gravitational waves, in a different manner.

Tews et al. (2018) critically examined this idea by using parameterized, general nuclear-matter equations of state. Their key finding is that the maximum mass is correlated only very weakly with binary tidal deformability for the masses consistent with GW170817. They found that some equations of state can support a neutron star with $>2.6\,M_\odot$ even if $\tilde{\Lambda}$ is significantly lower than 400. Because the remnant massive neutron star should survive for a very long time, or possibly

---

[7] More precisely, this threshold is derived by fitting the multi-color evolution of AT 2017gfo.

permanently, after merger for these cases (Hotokezaka et al. 2011, 2013a), the argument of Radice et al. (2018b) based on the mass of the ejecta cannot reject such equations of state and the binary tidal deformability. However, the maximum mass of a neutron star might also be constrained to $\lesssim 2.2\,M_\odot$ as described above. Whether this constraint on the maximum mass is compatible with the luminosity of AT 2017gfo is not trivial.

In this Letter, we demonstrate that the lower bound on $\tilde{\Lambda}$ is not as significant as what Radice et al. (2018b) proposed, even if the maximum mass is only moderately large, $M_{\rm max} \lesssim 2.1\,M_\odot$, by a suite of numerical-relativity simulations. Specifically, we find that various models with $\tilde{\Lambda} < 400$ can eject $0.05\,M_\odot$ and can explain the luminosity of AT 2017gfo. The models include asymmetric binary neutron stars with $\tilde{\Lambda} = 242$, which may not collapse at least until 20 ms after merger. In addition, we also show that the luminosity of AT 2017gfo could be explained even if the merger remnant does not experience bounce after merger, when the binary is asymmetric.

2. Model and Equation of State

We simulate mergers of equal-mass binaries with $1.375\,M_\odot$–$1.375\,M_\odot$ and unequal-mass binaries with $1.2\,M_\odot$–$1.55\,M_\odot$. The total mass, $m_0 = 2.75\,M_\odot$, and the mass ratios, $q = 1$ or 0.774, are consistent with GW170817 (Abbott et al. 2017c, 2019) and also with observed Galactic binary neutron stars (e.g., Tauris et al. 2017; Ferdman & PALFA Collaboration 2018). This should be contrasted with Radice et al. (2018b), where many models are significantly heavier than GW170817, particularly those with $\tilde{\Lambda} \lesssim 400$, and the mass ratio is restricted to $q > 0.857$. The initial orbital angular velocity Ω of the binary is chosen to be $Gm_0\Omega/c^3 \approx 0.025$ with applying eccentricity reduction (Kyutoku et al. 2014), where G and c are the gravitational constant and the speed of light, respectively. The binaries spend about six orbits before merger.

Equations of state for neutron star matter are varied systematically by adopting piecewise polytropes with three segments (Read et al. 2009). This choice allows us to investigate more generic models rather than particular nuclear-theory models, e.g., mean-field theory. The low-density segment is identical to that adopted in Hotokezaka et al. (2011). The middle-density segment is specified by pressure at $10^{14.7}\,{\rm g\,cm^{-3}}$ denoted by $P_{14.7}$ and an adiabatic index Γ. This segment is matched to the low-density part at the density where the pressure equals. The value of $P_{14.7}$ is known to be correlated with the neutron star radius (Lattimer & Prakash 2001; Read et al. 2009), and we choose $\log P_{14.7}$ (dyne cm^{-2}) from {34.1, 34.2, 34.3, 34.4, 34.5}. The value of Γ is determined by, in conjunction with the high-density segment, requiring the maximum mass of neutron stars to become $2.00\,M_\odot$, $2.05\,M_\odot$, and $2.10\,M_\odot$. The high-density segment is given by changing the adiabatic index to 2.8 at $10^{15}\,{\rm g\,cm^{-3}}$.

The first two columns of Table 1 list Γ and $P_{14.7}$ for the 14 equations of state[8] adopted in this study. The radius of a $1.35\,M_\odot$ neutron star and the maximum mass are shown in the third and fourth columns, respectively. We checked that all of them are causal; i.e., the sound velocity does not exceed c, up

to the central density of the spherical maximum mass configuration. Although our radii are typically smaller than those favored in Most et al. (2018), their probability distribution may be affected significantly by the small number of available equations of state with small radii (Raithel et al. 2018). As shown in Annala et al. (2018), our models are compatible with current understanding of nuclear physics and astronomical observations.

Table 1 also presents the binary tidal deformability of our equal-mass and unequal-mass binaries in the sixth column, where the mass ratio is given in the fifth column. All are consistent with constraints obtained by GW170817, irrespective of the details of the analysis (Abbott et al. 2017c, 2018, 2019; De et al. 2018). As pointed out by Tews et al. (2018), the binary tidal deformability is not directly correlated with the maximum mass.

3. Method of Simulations

Numerical simulations are performed in full general relativity with the SACRA code (Yamamoto et al. 2008; Kiuchi et al. 2017). The finite-temperature effect is incorporated by an ideal-gas prescription following Hotokezaka et al. (2011) with the fiducial value of $\Gamma_{\rm th} = 1.8$, which may be appropriate for capturing the dynamics of remnant neutron stars (Bauswein et al. 2010). We also performed simulations with $\Gamma_{\rm th} = 1.5$, 1.6, and 1.7 for some models with low values of $\tilde{\Lambda}$; the dependence of our results on $\Gamma_{\rm th}$ will be discussed. Because whether or not the merger remnant collapses into a black hole in a short timescale is important for this study, detailed physical effects such as magnetic fields and neutrino transport are neglected. They are known to play a central role on a longer timescale than durations of our simulations, which are performed until 10–20 ms after merger (Hotokezaka et al. 2013a); thus, our results should depend only weakly on these effects. Although we cannot determine the electron fraction of the ejecta, which is important to derive nucleosynthetic yields and characteristics of the kilonova/macronova (Wanajo et al. 2014; Kasen et al. 2017; Tanaka et al. 2017), it is not relevant to the purpose of this work.

We classify the fate of merger remnants into three types. If the remnant collapses into a black hole without experiencing bounce after merger, we call it a no-bounce collapse. Note that such collapses are denoted by the prompt collapse in Bauswein et al. (2017); we avoid this name, however, taking into account the fact that some asymmetric models survive longer than the dynamical timescale up to a few ms even if they do not experience bounce. If the remnant evades the no-bounce collapse but still collapses by 20 ms after merger, it is regarded as a short-lived remnant. This timescale is approximately identical to that adopted in Radice et al. (2018b). If the remnant massive neutron star does not collapse in our simulations, it is called a long-lived remnant. These three types will be denoted by "no bounce," "short," and "long" in Table 1, respectively.

We derive the baryonic mass of the unbound dynamical ejecta, $M_{\rm dyn}$, and that of the bound material outside the black hole or exceeding $10^{13}\,{\rm g\,cm^{-3}}$ for the long-lived remnant, $M_{\rm disk}$, from the simulations. The threshold density is chosen after Radice et al. (2018b), and the dependence of our results on this value will be described later. The ejecta as a whole should consist of the dynamical ejecta and the late-time outflow from the merger remnant (e.g., Fernández & Metzger 2013; Metzger & Fernández 2014; Just et al. 2015; Fujibayashi et al.

---

[8] We do not adopt ($\log P_{14.7}$, $M_{\rm max}$) = (34.5, $2.1 M_\odot$), because it is unnecessary for our purpose.

Table 1
Characteristic Quantities of Equations of State Adopted in this Work and Results of Simulations

Γ	$\log P_{14.7}$ (dyne cm^{-2})	$R_{1.35}$ (km)	M_{max} ($M_\odot$)	q	$\tilde{\Lambda}$	Type	M_{dyn} ($M_\odot$)	M_{disk} ($M_\odot$)	Δx (m)
3.765	34.1	10.4	2.00	1	208	no bounce	$<10^{-3}$	$<10^{-3}$	117
				0.774	218	no bounce	$<10^{-3}$	0.023	121
3.887	34.1	10.5	2.05	1	221	no bounce	$<10^{-3}$	$<10^{-3}$	118
				0.774	230	no bounce	5.2×10^{-3}	0.029	126
4.007	34.1	10.5	2.10	1	232	no bounce	1.9×10^{-3}	2.7×10^{-3}	118
				0.774	242	long	0.013	0.26 (0.16, 0.097)	121
3.446	34.2	10.6	2.00	1	232	no bounce	$<10^{-3}$	$<10^{-3}$	121
				0.774	245	no bounce	2.3×10^{-3}	0.036	124
3.568	34.2	10.7	2.05	1	247	no bounce	$<10^{-3}$	$<10^{-3}$	122
				0.774	259	no bounce	0.014	0.038	126
3.687	34.2	10.8	2.10	1	260	short	1.4×10^{-3}	7.8×10^{-3}	124
				0.774	272	long	0.011	0.26 (0.17, 0.092)	126
3.132	34.3	11.0	2.00	1	272	no bounce	$<10^{-3}$	$<10^{-3}$	126
				0.774	290	no bounce	0.012	0.063	131
3.252	34.3	11.1	2.05	1	288	no bounce	1.2×10^{-3}	1.9×10^{-3}	128
				0.774	305	short	0.015	0.12	131
3.370	34.3	11.1	2.10	1	303	short	2.0×10^{-3}	0.031	128
				0.774	319	long	0.011	0.25 (0.19, 0.12)	131
2.825	34.4	11.6	2.00	1	345	short	6.5×10^{-3}	0.018	134
				0.774	373	short	0.011	0.087	141
2.942	34.4	11.6	2.05	1	362	short	2.5×10^{-3}	0.016	134
				0.774	387	short	0.011	0.12	139
3.058	34.4	11.6	2.10	1	377	long	9.7×10^{-3}	0.17 (0.13, 0.11)	134
				0.774	400	short	9.0×10^{-3}	0.16	139
2.528	34.5	12.5	2.00	1	508	short	9.4×10^{-3}	0.053	149
				0.774	558	short	5.6×10^{-3}	0.16	156
2.640	34.5	12.4	2.05	1	516	short	0.012	0.12	147
				0.774	560	short	6.4×10^{-3}	0.18	154

Note. The first and second columns show the parameters that specify an equation of state, Γ and $\log P_{14.7}$, respectively. The third and fourth columns show the circumferential radius of a 1.35 $M_\odot$ neutron star $R_{1.35}$ and the maximum mass M_{max}, respectively. The next five columns present models of binaries and results of simulations, where the upper and lower rows correspond to equal-mass and unequal-mass binaries, respectively. The values of the mass ratio q and binary tidal deformability $\tilde{\Lambda}$ are given in the fifth and sixth columns, respectively. The seventh, eighth, and ninth columns show the fate of the remnant, the mass of dynamical ejecta M_{dyn}, and the mass of the bound material outside the black hole or exceeding 10^{13} g cm^{-3} for the long-lived remnant M_{disk}, for our fiducial $\Gamma_{th} = 1.8$. For the long-lived remnants, we also show M_{disk} for the threshold density 10^{12} and 10^{11} g cm^{-3} in the parentheses. The fate is classified into the collapse without bounce (no bounce), the short-lived remnant (short), and the long-lived remnant (long) as defined in the body text. The tenth column shows the grid spacing Δx in the finest domain.

2018). Because our simulations do not include magnetic fields or corresponding viscosity required to launch the outflow, we simply assume that some fraction of M_{disk} will be ejected by such processes following Radice et al. (2018b). While Radice et al. (2018b) conservatively (for their purpose) adopted 100% efficiency for the ejection from the accretion torus, this efficiency is likely to be lower than 50%, particularly when the remnant is a black hole, because the outflow is a result of the accretion.

Our results depend weakly on grid resolutions as shown in Table 2. By simulating selected models with three different resolutions, we estimate that the mass of the ejecta has a relative error of about a factor of two and an absolute error of $10^{-3} M_\odot$ for typical cases with hypothetical first-order convergence. However, the nominal error reaches an order of magnitude for marginally stable short-lived remnants, because the fate wanders from the no-bounce collapse to the short-lived remnant. We think that this is reasonable and inevitable for models near the threshold, and these errors should be kept in mind when we discuss implications to AT 2017gfo. In the rest of this Letter, we only show the results of highest-resolution runs, in which the neutron star radius is covered by ≈65–70 points with the grid spacing at the finest domain shown in the tenth column of Table 1.

4. Result

The merger of binary neutron stars results in dynamical mass ejection and the formation of a remnant, a massive neutron star or a black hole, surrounded by an accretion torus. Because their dynamics and mechanisms have been thoroughly described in previous publications (e.g., Bauswein et al. 2013; Hotokezaka et al. 2013b; Radice et al. 2016), we do not repeat detailed explanations. The fate of the merger remnant (seventh column), the mass of the dynamical ejecta (eighth column), and the mass of the bound material outside the black hole or exceeding 10^{13} g cm^{-3} for the long-lived remnant (ninth column) are presented in Table 1. The mass of the bound material, M_{disk}, for a given equation of state is usually larger for unequal-mass binaries rather than for equal-mass binaries because of the efficient tidal interaction and angular momentum transfer during merger. In particular, some of the asymmetric models leave a baryonic mass of $\gtrsim 0.03\,M_\odot$ even for the no-bounce collapse. This is because the light components are deformed significantly before merger and the collapses are gradually induced by the accretion for these models (see http://www2.yukawa.kyoto-u.ac.jp/~kenta.kiuchi/GWRC/index.html for visualization).

Table 2
Dependence of the Fate of the Remnant, M_{dyn}, and M_{disk} on the Grid Spacing, Δx

q	$\tilde{\Lambda}$	Δx (m)	Type	M_{dyn} ($M_{\odot}$)	M_{disk} ($M_{\odot}$)
1	288	128	no bounce	1.2×10^{-3}	1.9×10^{-3}
		148	no bounce	2.1×10^{-3}	4.8×10^{-3}
		164	short	6.9×10^{-3}	0.013
1	508	149	short	9.4×10^{-3}	0.053
		172	short	0.011	0.055
		191	short	8.5×10^{-3}	0.045
1	516	147	short	0.012	0.12
		170	short	0.013	0.089
		189	short	0.012	0.095
0.774	242	121	long	0.013	0.26
		140	long	0.017	0.26
		156	long	0.019	0.25
0.774	259	128	no bounce	0.014	0.038
		148	no bounce	0.014	0.041
		164	short	0.015	0.31
0.774	290	131	no bounce	0.012	0.063
		152	no bounce	0.013	0.063
		169	no bounce	0.014	0.069
0.774	558	156	short	5.6×10^{-3}	0.16
		180	short	4.7×10^{-3}	0.14
		201	short	4.5×10^{-3}	0.16
0.774	560	154	short	6.4×10^{-3}	0.18
		178	short	5.5×10^{-3}	0.19
		198	short	5.4×10^{-3}	0.15

Note. We specify the models by q and $\tilde{\Lambda}$ to be compared with those shown in Table 1.
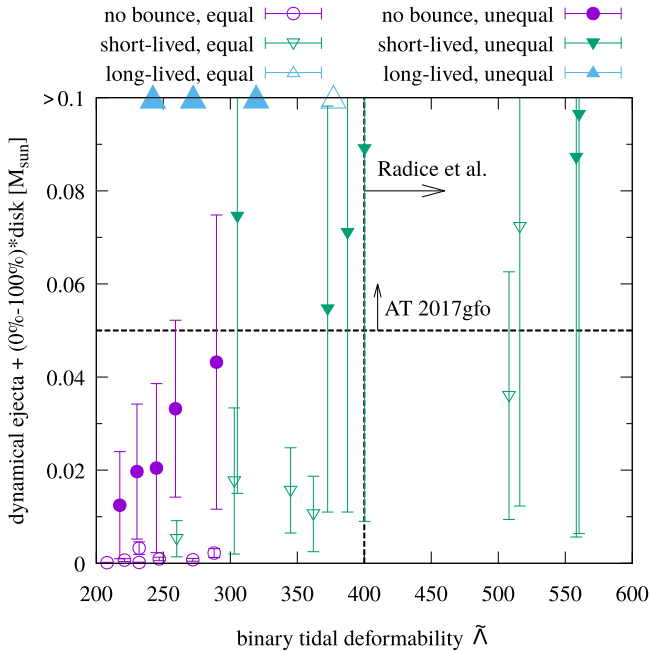
Figure 1. Mass of the ejecta vs. the binary tidal deformability. The errorbars indicate ejection of the remnant by from 0% (i.e., only dynamical mass ejection occurs) to 100% (i.e., all the mass outside the black hole is ejected), and the 50% ejection of the baryonic mass surrounding the black hole is marked with symbols. Open and filled symbols denote equal-mass and unequal-mass models, respectively. Large triangles on the top axis denote the models for which remnant massive neutron stars survive longer than 20 ms, and thus the luminosity of AT 2017gfo can be explained. Such a model is found even at $\tilde{\Lambda} = 242$. The vertical dashed line at $\tilde{\Lambda} = 400$ is the threshold proposed by Radice et al. (2018b). The horizontal dashed line at 0.05 $M_{\odot}$ indicates the mass required to explain AT 2017gfo (Radice et al. 2018b).
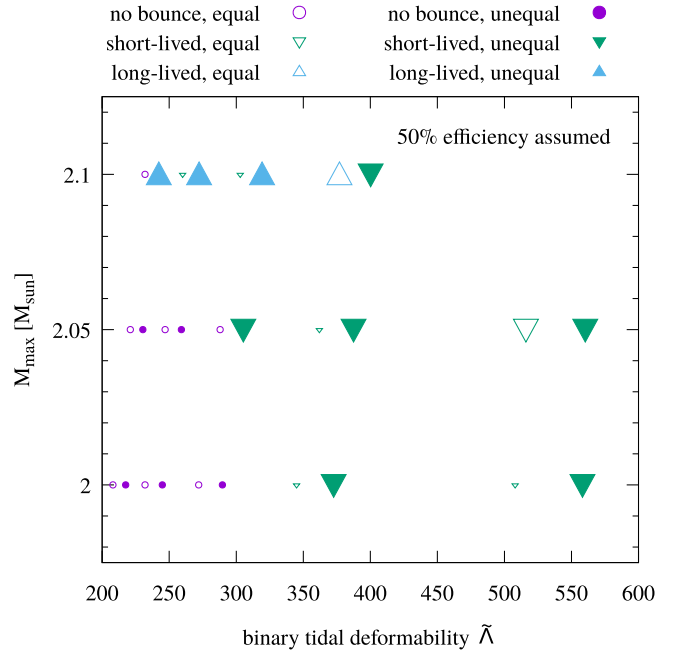

Figure 2. Summary of whether the luminosity of AT 2017gfo can be explained by each model in the binary tidal deformability ($\tilde{\Lambda}$)-maximum mass (M_{max}) plane. The large symbols denote models that can eject 0.05 $M_{\odot}$ with hypothetical 50% efficiency and can explain the luminosity of AT 2017gfo, and the small ones denote those that cannot.

The masses of the ejecta are summarized visually in Figure 1 against the binary tidal deformability, $\tilde{\Lambda}$. It is obvious that many binary models with $\tilde{\Lambda} < 400$ can eject more than 0.05 $M_{\odot}$ and are capable of explaining the luminosity of AT 2017gfo as far as the mass of the ejecta is concerned. Indeed, we find that a handful of binary models with $\tilde{\Lambda} < 400$ result in the formation of a long-lived remnant, for which M_{disk} is always larger than 0.1 $M_{\odot}$. We have verified that the luminosity of AT 2017gfo can be explained with 50% ejection efficiency even if the threshold density is decreased to 10^{11} g cm^{-3} (see Table 1). They serve as counterexamples to the claim that $\tilde{\Lambda} \gtrsim 400$ is required to explain AT 2017gfo (Radice et al. 2018b).

The key ingredients are the not-so-small maximum mass, M_{max}, and the mass asymmetry represented by the small mass ratio, q. Their importance is understood from Figure 2, where we summarize which model can explain the luminosity of AT 2017gfo in the $\tilde{\Lambda}$–M_{max} plane. Here, we assume a 50% ejection efficiency of the bound material for concreteness. On the one hand, for the case that the maximum mass is $2\,M_{\odot}$, all the models collapse by 20 ms after merger. Equal-mass models have no chance of ejecting 0.05 $M_{\odot}$,[9] and the mass asymmetry of $q = 0.774$ does not save any model with $\tilde{\Lambda} < 377$. On the other hand, if the maximum mass is as large as 2.1 $M_{\odot}$, many models produce long-lived remnants. Actually, all the asymmetric binaries considered here are capable of explaining the luminosity of AT 2017gfo. The lowest value of $\tilde{\Lambda}$ of models that can eject 0.05 $M_{\odot}$ is 242. Figure 2 suggests that, if M_{max} is larger than 2.1 $M_{\odot}$, then the lower bound on $\tilde{\Lambda}$ derived by AT 2017gfo may become looser than that found in this study.

---

9 A model with $\tilde{\Lambda} = 508$ can eject 0.05 $M_{\odot}$ if the efficiency exceeds 77%.

Table 3
Dependence of the Fate of the Remnant, M_{dyn}, and M_{disk} on Γ_{th}

q	$\tilde{\Lambda}$	Γ_{th}	Type	M_{dyn} ($M_\odot$)	M_{disk} ($M_\odot$)
0.774	242	1.8	long	0.013	0.26
		1.7	short	0.011	0.045
		1.6	short	7.6×10^{-3}	0.036
		1.5	short	6.5×10^{-3}	0.033
0.774	272	1.8	long	0.011	0.26
		1.7	long	0.013	0.26
		1.6	long	0.014	0.27
		1.5	short	9.8×10^{-3}	0.042

Note. We specify the models by $q(=0.774)$ and $\tilde{\Lambda}$ to be compared with those shown in Table 1.

We also find that all the models with $\tilde{\Lambda} > 400$ are capable of ejecting $0.05\,M_\odot$ if 100% ejection efficiency is adopted. This is consistent with the findings of Radice et al. (2018b).

The fate of the merger remnant depends on the strength of the finite-temperature effect for marginal cases. For example, the lowest value of $\tilde{\Lambda}$ that can explain the luminosity of AT 2017gfo is 242 in our models if the fiducial $\Gamma_{th} = 1.8$ is adopted, where the outcome is a long-lived remnant. However, the remnant becomes short lived for $\Gamma_{th} \leqslant 1.7$ because of the reduced thermal pressure and fails to eject $0.05\,M_\odot$. This indicates that the finite-temperature effect must be moderately strong for this model to account for AT 2017gfo. We also find that the model with $\tilde{\Lambda} = 272$ results in the long-lived remnant only when $\Gamma_{th} \geqslant 1.6$, whereas the short-lived remnant for a very small value of $\Gamma_{th} = 1.5$ can eject $0.05\,M_\odot$ if 100% efficiency is assumed. The results for are summarized in Table 3. Although our conclusion that binaries with $\tilde{\Lambda} \lesssim 400$ are capable of explaining the luminosity of AT 2017gfo is unchanged, these observations imply that accurate incorporation of the finite-temperature effect is also crucial to infer precise properties of the zero-temperature equation of state from electromagnetic counterparts.

5. Discussion

We conclude that the lower bound on binary tidal deformability is $\tilde{\Lambda} \leqslant 242$ if an ejection of $0.05\,M_\odot$ is required. We speculate that lower values of $\tilde{\Lambda}$ than this could even be acceptable if we employ an equation of state that supports a maximum mass larger than $2.1\,M_\odot$ and/or increase the degree of asymmetry. The precise value of the threshold depends also on the strength of the finite-temperature effect, represented by Γ_{th} in our study.

We also find that an asymmetric binary that results in a no-bounce collapse can explain the luminosity of AT 2017gfo, if moderately high $\approx 60\%$ ejection efficiency from the remnant is admitted. The lower bounds proposed in Bauswein et al. (2017) are satisfied for the equation of state of this model, with which the radii of $1.6\,M_\odot$ and maximum-mass configurations are 10.93 and 9.66 km, respectively. However, our finding would potentially invalidate the argument of Bauswein et al. (2017) and its future application.

Our results indicate that the mass ratio is critically important to derive reliable constraints on neutron star properties from electromagnetic emission as also argued in Radice et al. (2018b). If the binary turns out to be symmetric, it is possible that $\tilde{\Lambda} \gtrsim 400$ is necessary as Radice et al. (2018b) originally
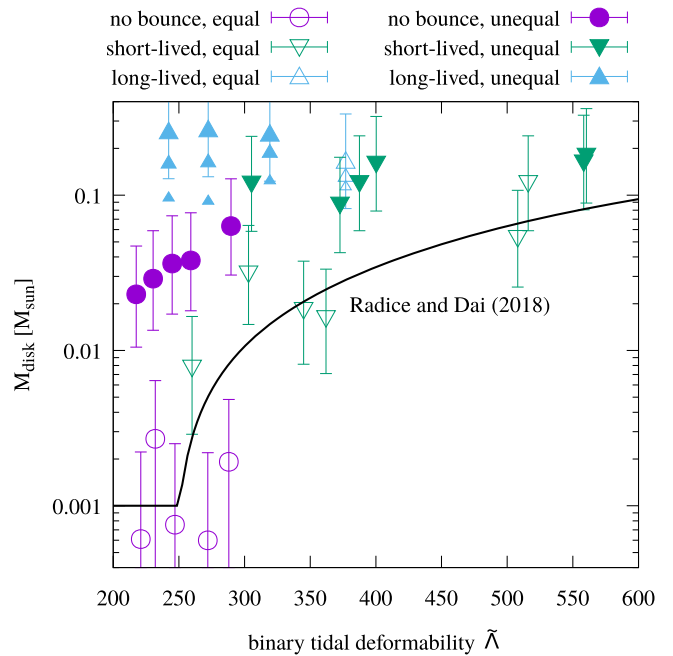

Figure 3. Disk mass vs. the binary tidal deformability. The errorbars denote the typical relative error of a factor of two and absolute error of $10^{-3}\,M_\odot$ (see Section 3). The values for the threshold density of $10^{12}\,{\rm g\,cm}^{-3}$ and $10^{11}\,{\rm g\,cm}^{-3}$ are shown with small symbols for long-lived remnants. We also show the fit derived in Radice & Dai (2019). The correlation between M_{disk} and $\tilde{\Lambda}$ is not significant in our models, and the applicability of the fit due to Radice & Dai (2019) is very limited.

proposed. Indeed, we find no symmetric model with $\tilde{\Lambda} < 377$ that can eject $0.05\,M_\odot$. However, Figure 3 shows that the mass asymmetry significantly obscures the correlation between the disk mass and binary tidal deformability, which is the basis of previous attempts to constrain $\tilde{\Lambda}$ from AT 2017gfo. In light of our results, fitting formulas adopted in Radice & Dai (2019) and Coughlin et al. (2018a) have severe systematic errors. Further investigation is required to clarify precisely the effect of asymmetry. Although the mass ratio can be determined from gravitational-wave data analysis, the degeneracy with the spin must be resolved to achieve high precision (Hannam et al. 2013).

The velocity and the composition can potentially be used as additional information to examine binary models. Some previous work attempted to associate either the blue or red component of AT 2017gfo to dynamical ejecta to improve parameter estimation (Gao et al. 2017; Coughlin et al. 2018b). However, the derived binary parameters, in particular the mass ratio, disagree between these works. As shown by Kawaguchi et al. (2018), such an association is not necessarily justified once interaction among multiple ejecta components is taken into account. Detailed modelings of the emission are required if we would like to utilize the velocity and/or the composition to put constraints on properties of neutron stars.

Another lesson drawn from our study is that the possible parameter space of nuclear physics may not be satisfactorily covered by current tabulated equations of state (Tews et al. 2018). For example, equations of state derived by relativistic mean-field theory tend to predict a large maximum mass only when the typical radius is large (Radice et al. 2018a), and thus the value of binary tidal deformability is also high. Such a correlation is not likely to be physical but ascribed to the method of quantum many-body calculations. Specifically, the

large maximum mass and the small radius can be accommodated in variational calculations (e.g., Togashi et al. 2017). As Figure 2 shows, the outcome of the merger depends significantly on the maximum mass, even if the binary tidal deformability is unchanged. It should be remarked that models with $\tilde{\Lambda} < 400$ of Radice et al. (2018b) are generated by assigning total masses larger than those allowed by GW170817 (Abbott et al. 2017c, 2019) except for the SFHo equation of state (Steiner et al. 2013). It is impossible for other equations of state adopted by them to produce binary models equipped with $\tilde{\Lambda} \lesssim 400$ and the total mass allowed by GW170817 simultaneously. This feature artificially enhances the chance of the early collapse. If we wish to put reliable constraints on neutron stars via numerical simulations, care must be taken regarding the limitation of the adopted models including the finite-temperature effect.

ORCID iDs

Kenta Kiuchi ⓘ https://orcid.org/0000-0003-4988-1438
Koutarou Kyutoku ⓘ https://orcid.org/0000-0003-3179-5216
Masaru Shibata ⓘ https://orcid.org/0000-0002-4979-5671

References

Abbott, B. P., Abbott, R., Abbott, T. D., et al. 2017a, Natur, 551, 85
Abbott, B. P., Abbott, R., Abbott, T. D., et al. 2017b, ApJL, 848, L13
Abbott, B. P., Abbott, R., Abbott, T. D., et al. 2017c, PhRvL, 119, 161101
Abbott, B. P., Abbott, R., Abbott, T. D., et al. 2017d, ApJL, 848, L12
Abbott, B. P., Abbott, R., Abbott, T. D., et al. 2018, PhRvL, 121, 161101
Abbott, B. P., Abbott, R., Abbott, T. D., et al. 2019, PhRvX, 9, 011001
Annala, E., Gorda, T., Kurkela, A., & Vuorinen, A. 2018, PhRvL, 120, 172703
Bauswein, A., Goriely, S., & Janka, H.-T. 2013, ApJ, 773, 78
Bauswein, A., Janka, H.-T., & Oechslin, R. 2010, PhRvD, 82, 084043
Bauswein, A., Just, O., Janka, H.-T., & Stergioulas, N. 2017, ApJL, 850, L34
Burgio, G. F., Drago, A., Pagliara, G., Schulze, H.-J., & Wei, J.-B. 2018, ApJ, 860, 139
Coughlin, M. W., Dietrich, T., Margalit, B., & Metzger, B. D. 2018a, arXiv:1812.04803
Coughlin, M. W., Dietrich, T., Doctor, Z., et al. 2018b, MNRAS, 480, 3871
De, S., Finstad, D., Lattimer, J. M., et al. 2018, PhRvL, 121, 091102
Ferdman, R. D. & PALFA Collaboration 2018, in IAU Symp. 337, Pulsar Astrophysics the Next Fifty Years, ed. P. Weltevrede (Cambridge: Cambridge Univ. Press), 146
Fernández, R., & Metzger, B. D. 2013, MNRAS, 435, 502
Fujibayashi, S., Kiuchi, K., Nishimura, N., Sekiguchi, Y., & Shibata, M. 2018, ApJ, 860, 64
Gao, H., Cao, Z., Ai, S., & Zhang, B. 2017, ApJL, 851, L45
Hannam, M., Brown, D. A., Fairhurst, S., Fryer, C. L., & Harry, I. W. 2013, ApJL, 766, L14
Hotokezaka, K., Kiuchi, K., Kyutoku, K., et al. 2013a, PhRvD, 88, 044026
Hotokezaka, K., Kiuchi, K., Kyutoku, K., et al. 2013b, PhRvD, 87, 024001
Hotokezaka, K., Kyutoku, K., Okawa, H., Shibata, M., & Kiuchi, K. 2011, PhRvD, 83, 124008
Just, O., Bauswein, A., Pulpillo, R. A., Goriely, S., & Janka, H.-T. 2015, MNRAS, 448, 541
Kasen, D., Metzger, B., Barnes, J., Quataert, E., & Ramirez-Ruiz, E. 2017, Natur, 551, 80
Kawaguchi, K., Shibata, M., & Tanaka, M. 2018, ApJL, 865, L21
Kiuchi, K., Kawaguchi, K., Kyutoku, K., et al. 2017, PhRvD, 96, 084060
Kyutoku, K., Shibata, M., & Taniguchi, K. 2014, PhRvD, 90, 064006
Lattimer, J. M., & Prakash, M. 2001, ApJ, 550, 426
Lim, Y., & Holt, J. W. 2018, PhRvL, 121, 062701
Malik, T., Alam, N., Fortin, M., et al. 2018, PhRvC, 98, 035804
Margalit, B., & Metzger, B. D. 2017, ApJL, 850, L19
Metzger, B. D., & Fernández, R. 2014, MNRAS, 441, 3444
Mooley, K. P., Deller, A. T., Gottlieb, O., et al. 2018, Natur, 561, 355
Most, E. R., Weih, L. R., Rezzolla, L., & Schaffner-Bielich, J. 2018, PhRvL, 120, 261103
Radice, D., & Dai, L. 2019, EPJA, 55, 50
Radice, D., Galeazzi, F., Lippuner, J., et al. 2016, MNRAS, 460, 3255
Radice, D., Perego, A., Hotokezaka, K., et al. 2018a, ApJ, 869, 130
Radice, D., Perego, A., Zappa, F., & Bernuzzi, S. 2018b, ApJL, 852, L29
Raithel, C. A., Özel, F., & Psaltis, D. 2018, ApJL, 857, L23
Read, J. S., Lackey, B. D., Owen, B. J., & Friedman, J. L. 2009, PhRvD, 79, 124032
Rezzolla, L., Most, E. R., & Weih, L. R. 2018, ApJL, 852, L25
Ruiz, M., Shapiro, S. L., & Tsokaros, A. 2018, PhRvD, 97, 021501
Shibata, M., Fujibayashi, S., Hotokezaka, K., et al. 2017, PhRvD, 96, 123012
Steiner, A. W., Hempel, M., & Fischer, T. 2013, ApJ, 774, 17
Tanaka, M., Utsumi, Y., Mazzali, P., et al. 2017, PASJ, 69, 102
Tauris, T. M., Kramer, M., Freire, P. C. C., et al. 2017, ApJ, 846, 170
Tews, I., Margueron, J., & Reddy, S. 2018, PhRvC, 98, 045804
Togashi, H., Nakazato, K., Takehara, Y., et al. 2017, NuPhA, 961, 78
Wanajo, S., Sekiguchi, Y., Nishimura, N., et al. 2014, ApJL, 789, L39
Yamamoto, T., Shibata, M., & Taniguchi, K. 2008, PhRvD, 78, 064054
Zhao, T., & Lattimer, J. M. 2018, PhRvD, 98, 063020